



**HAL**  
open science

## **Always remain suspicious: a case study on tracking down a technical artefact while measuring IR-RF**

Sebastian Kreutzer, Madhav Krishna Murari, Marine Frouin, Markus Fuchs,  
Norbert Mercier

► **To cite this version:**

Sebastian Kreutzer, Madhav Krishna Murari, Marine Frouin, Markus Fuchs, Norbert Mercier. Always remain suspicious: a case study on tracking down a technical artefact while measuring IR-RF. *Ancient TL*, 2017, 35 (1), pp.20-30. hal-01846143

**HAL Id: hal-01846143**

**<https://hal.science/hal-01846143>**

Submitted on 27 Jul 2018

**HAL** is a multi-disciplinary open access archive for the deposit and dissemination of scientific research documents, whether they are published or not. The documents may come from teaching and research institutions in France or abroad, or from public or private research centers.

L'archive ouverte pluridisciplinaire **HAL**, est destinée au dépôt et à la diffusion de documents scientifiques de niveau recherche, publiés ou non, émanant des établissements d'enseignement et de recherche français ou étrangers, des laboratoires publics ou privés.

## Always remain suspicious: a case study on tracking down a technical artefact while measuring IR-RF

Sebastian Kreutzer<sup>1</sup>, Madhav Krishna Murari<sup>2</sup>, Marine Frouin<sup>3</sup>  
Markus Fuchs<sup>2</sup>, Norbert Mercier<sup>1</sup>

<sup>1</sup>IRAMAT-CRP2A, Université Bordeaux Montaigne, Pessac Cedex, France

<sup>2</sup>Department of Geography, Justus-Liebig-University Giessen, Germany

<sup>3</sup>Research Laboratory for Archaeology and the History of Art, Oxford University, Oxford, United Kingdom

\* Corresponding Author: sebastian.kreutzer@u-bordeaux-montaigne.fr

Received: March 22, 2017; in final form: June 13, 2017

### Abstract

Identifying systematic errors that are introduced by the measurement equipment is a necessary prerequisite for reproducible measurements and reliable results. However, technical artefacts often remain unpublished. Here we report on a sudden change of luminescence intensity observed while measuring IR-RF signals from K-feldspar extracts. The measurements were carried out on a *lexsyg research* reader. A lateral movement of the sample carrier up to 0.5 mm relative to the photomultiplier tube and the irradiation source, causes a change in the sample geometry. This movement results in inter-aliquot scatter during the measurement of IR-RF. Two solutions are discussed to remove this effect: (I) data post-processing and (II) design change by the manufacturer. Our study so far is limited to IR-RF measurements on a single luminescence reader and suggests due caution in the identification of such systematic errors.

**Keywords:** Luminescence, Infrared Radiofluorescence, Instrumentation

### 1. Introduction

It is assumed that the measured data are free from systematic errors caused by the instrument design. To identify and quantify the potential sources of systematic errors, measurement equipment is often tested rigorously before its routine use (e.g., Lomax et al., 2014). However, several sources of systematic errors do not necessarily reveal themselves during

routine measurements. Some require time-consuming tests (e.g., Bray et al., 2002; Adamiec et al., 2011; Schmidt et al., 2011; Kadereit & Kreutzer, 2013) and the magnitude of the error may depend on the technical design (Kreutzer et al., 2013). Such errors often result in scattered data which hampers their direct discovery. Besides, the scatter might make publication difficult; the issue remains unreported and thus might be repeated by other groups.

At the IRAMAT-CRP2A in Bordeaux (France) several studies on infrared radiofluorescence (IR-RF) of potassium-enriched feldspar (K-feldspar) extracts have been undertaken since 2012. The IR-RF signal of K-feldspar is believed to provide a promising alternative to the so far established luminescence dating approaches, e.g., quartz SAR protocol (Murray & Wintle, 2000) or post-IR IRSL on feldspar (Thomsen et al., 2008). The IR-RF technique was introduced by Trautmann et al. (1999) and Erfurt & Krbetschek (2003) and later successfully applied by, e.g., Wagner et al. (2010). In contrast, Buylaert et al. (2012) raised considerable doubts on the applicability of the method for age determinations. Re-investigation of the IR-RF signal characteristics at the IRAMAT-CRP2A recently led to an improved protocol that uses stimulation at a higher temperature (here 70 °C instead of room temperature) for recording the IR-RF signal (Frouin, 2014; Frouin et al., 2015; Huot et al., 2015; Frouin et al., 2017).

While conducting further methodological studies using fine grain (4-11 µm, gently crushed coarse grains) K-feldspar separates, we encountered an unexpected inter-aliquot scatter (Kreutzer, 2016). Such scatter was previously reported by Krbetschek et al. (2000) and later by Frouin et al. (2017) on coarse grains (100-200 µm) and has been interpreted as being due to variations in the properties of the individual grains and/or superposition of competing signals. When measuring the fine grain fraction (ca. 10<sup>6</sup> grains/cup) a low scatter is

expected due to signal averaging effects. However, to our surprise, we observed a high inter-aliquot scatter. The observation gave rise to the idea that the measurement device might cause this variation.

Here we report on a series of instrumental tests performed on a particular Freiberg Instruments *lexsyg research* reader (Richter et al., 2013) at the IRAMAT-CRP2A. We present a case study to track down a repetitive, unwanted effect on this device. Our contribution continues a discussion initiated at the German LED 2016 in Emmendingen (Kreutzer, 2016).

## 2. Measurement setup

Measurements were carried out on a Freiberg Instruments *lexsyg research* reader (Richter et al., 2013) at the IRAMAT-CRP2A, Bordeaux (reader id: 12-re-01-0007). The device is equipped with a  $^{90}\text{Sr}/^{90}\text{Y}$  ring-source (Richter et al., 2012). For IR-RF signal detection a Chroma D850/40 interference filter was used in front of a Hamamatsu H7421-50 PMT. For bleaching, we used the built-in solar simulator (SLS). The SLS is equipped with LEDs comprising six different wavelengths (cf. Frouin et al., 2017). All bleaching and measurement settings followed the suggestions made by Frouin et al. (2017). Relevant protocol parameters are listed below.

The samples (BDX16646, BDX16650, BDX16651) used for the experiments originate from the Atlantic coast (Médoc) in the north-west of Bordeaux (France). Sample preparation was carried out using routine methods for preparing coarse grain feldspar samples (e.g., Preusser et al., 2008). The grain size of 100–200  $\mu\text{m}$  was extracted by wet sieving. Chemical treatments comprised, HCl (10%),  $\text{H}_2\text{O}_2$  (30%), LST heavy liquids (2.72  $\text{g cm}^{-3}$ , 2.62  $\text{g cm}^{-3}$ , 2.58  $\text{g cm}^{-3}$ ). The K-feldspar fraction was not further etched. The fine grain fraction (4–11  $\mu\text{m}$ ) was obtained by gentle crushing of the coarse grains with a mortar and applying the Stokes' law. Approximately 0.6 mg of sample material were settled on austenitic stainless steel cups<sup>1</sup> delivered by Freiberg Instruments. All measurements were done in air.

The data analysis was carried out using the **R** package 'Luminescence' (Kreutzer et al., 2012, 2017).

## 3. Identifying an artefact

In the following section, we describe two independent IR-RF experiments that raised our suspicions about the reliability of the measurement equipment.

### 3.1. Experiment I

Our measurement protocol, henceforth called  $\text{RF}_{70}$ , is based on the IRSAR protocol by Erfurt & Krbetschek (2003); further developed by Frouin et al. (2017). It was applied to the fine-grained K-feldspar (FG-KFS) fraction of sample BDX16646. The  $\text{RF}_{70}$  protocol consists of two IR-RF steps (natural: 3,600 s and regenerative: 10,000 s) separated by a

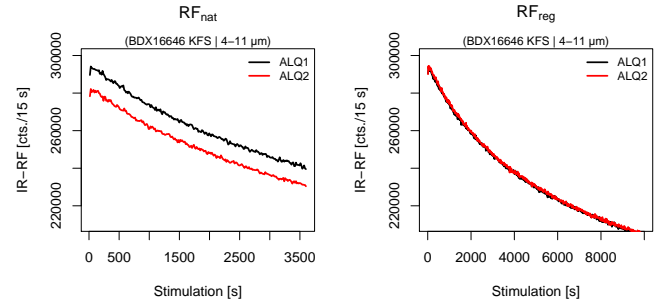


Figure 1. Results of  $\text{RF}_{70}$  measurements of sample BDX16646 after bleaching for 10,000 s. Two aliquots were measured. The left plot shows the natural IR-RF ( $\text{RF}_{\text{nat}}$ ) curves, the right plot the regenerated IR-RF ( $\text{RF}_{\text{reg}}$ ) curves. Please note that 'natural' here refers to the IRSAR and  $\text{RF}_{70}$  protocol nomenclature, indicating the first of the two measured IR-RF curves. For further details see main text.

bleaching (10,000 s) and a pause (3,600 s). Due to an artificial bleaching prior to the measurements (bleaching settings according to Frouin et al. 2017), the expected residual dose was supposed to be zero for both aliquots. The pause between the preceding artificial bleaching and the measurement was up to 2 days. The results of the measurements are shown in Fig. 1. Both regenerated IR-RF curves ( $\text{RF}_{\text{reg}}$ ) are similar in shape and intensity (right plot). In contrast, the reset ('natural') IR-RF ( $\text{RF}_{\text{nat}}$ ) curves (left plot), differ by ca. 4% in their maximum intensity. Please note that, even the  $\text{RF}_{\text{nat}}$  was artificially bleached before measurement, we chose the term  $\text{RF}_{\text{nat}}$  for consistency with the published literature.

The equivalent doses ( $D_e$ ) for the two aliquots were estimated with the horizontal sliding approach (Frouin et al. (2017)) and resulted in apparent doses of 0.9 { $Q_{2.5}$ : -0.9 ;  $Q_{97.5}$ : 2.7} Gy (black curve) and 49.5 { $Q_{2.5}$ : 45.0 ;  $Q_{97.5}$ : 54} Gy (red curves).<sup>2</sup> These results are unexpected for two reasons: (1) Due to the amount of grains (ca.  $10^6$ ) on each cup the inter-aliquot scatter was expected to be negligible and (2) the apparent dose should be approx. 0 Gy for both aliquots. In other words, the maximum  $\text{RF}_{\text{nat}}$  signal intensity difference of ca. 4%, results in an apparent dose ca. 55 times higher for the second aliquot in comparison to the first aliquot.

Frouin et al. (2017) (supplement) showed that the relation between  $\text{RF}_{\text{nat}}$  and  $\text{RF}_{\text{reg}}$  can be written as

$$\text{RF}_{\text{nat}}(t) = \text{RF}_{\text{reg}}(t + t_n) + \varepsilon_t$$

where  $\varepsilon_t$  is the residual signal at time  $t$  within the co-domain  $t \in \{t_{\min}, \dots, t_{\text{natmax}}\}$ . The simplification considers  $\text{RF}_{\text{nat}}$  to be an extract of  $\text{RF}_{\text{reg}}$ . Since the  $\text{RF}_{\text{nat}}$  curves in Fig. 1 (left) have different intensities, one would expect that they represent sections of the  $\text{RF}_{\text{reg}}$  curves in Fig. 1 (right). Hence, the red curve would have a flatter slope plotted than the normalised curve shows. Nevertheless, the normalised curves shown in Fig. 2 (left) reveal that both  $\text{RF}_{\text{nat}}$  curves have a similar shape leading to the speculation whether the determined dose is a measurement artefact.

<sup>1</sup>VA steal, quality: X15CrNiSi25-21, number: 1.4841, inner diameter: 7.95 mm, outer diameter: 9.95 mm, thickness bottom: 0.49 mm

<sup>2</sup>The terms  $Q_{2.5}$  and  $Q_{97.5}$  refer to the lower 2.5% and the upper 97.5% quantiles, respectively.

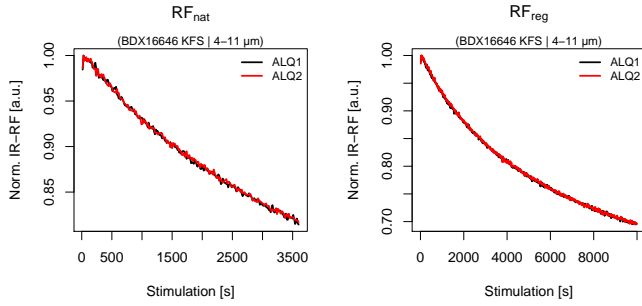


Figure 2. Similar as in Fig. 1, but with curves being normalised to the highest count value of each IR-RF curve.

### 3.2. Experiment II

The second experiment originally aimed at investigating potential short-time fading. The question whether the IR-RF suffers from anomalous fading (Wintle, 1973) is controversial and is discussed in the literature (e.g., Buylaert et al., 2012). However, so far no evidence for fading of the IR-RF signal has been presented. The sequence described in Table 1 aimed at detecting any short-term fading. The sequence consists of three steps: A pause of 3,600 s interspersed two IR-RF steps carried out at the SLS position (without bleaching).

Table 1. Measurement sequence used to investigate the short-term fading of the  $RF_{70}$  signal.

#	Step	Pos.	Obs.
1	Bleaching at 70 °C for 10,800 s	SLS	-
2	IR-RF measurements for 1,000 s at 70 °C after a stabilisation period of 900 s, channel resolution 15 s/channel	$\beta$ -source	IR-RF
3	Pause for 3,600 s	SLS	-
4	Return to step 2	-	-

Four aliquots of the FG-KFS sample BDX16650 were measured. The sample was used in previous experiments with negligible sensitivity change. First, any residual signal was reset using the bleaching settings by Frouin et al. (2017) (Table 1, step 1). The full sequence was repeated three times for each aliquot.

The results for the four aliquots (represented by different colours) are shown in Fig. 3. Line styles indicate repeated cycles for the same aliquot. The pause of 3,600 s is indicated in the figure (please note the gap in the scale for the x-axis).

Figure 3 shows that (1) the IR-RF signals differ considerably between aliquots, which indicates that the observation made in Fig. 1 (similarity of the  $RF_{reg}$  of two aliquots) was coincidence, since this pattern could not be reproduced. (2) Although the general curve shapes appear similar, the intensities vary randomly with repetition. (3) The IR-RF signal after the pause is in two out of twelve cases higher (red circle) and for the remaining cases lower than the IR-RF signal before the pause. If the IR-RF signal of this particular sample did suffer from fading, the IR-RF signal after the

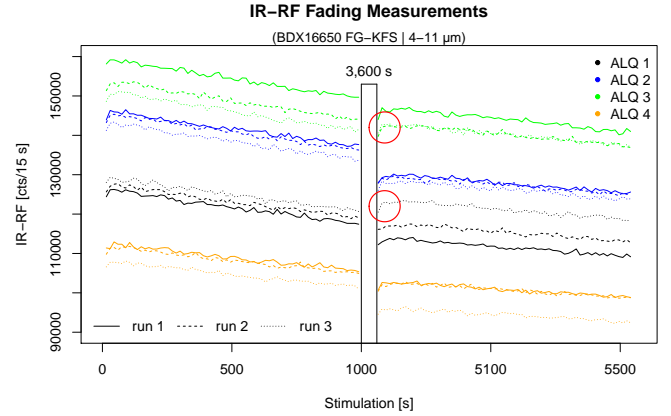


Figure 3. Fading measurements of the fine grain KFS fraction of sample BDX16650. IR-RF signals are recorded for 1000 s (ca. 60 Gy), with a pause of 3,600 s in between. The two red circles mark higher IR-RF signals after the pause. Colours code aliquots, line styles run numbers (repetitions). The solid lines represent the first series of measurements. The sample arm moved between each step. For further details see main text.

pause would be higher in all cases. Nevertheless, the results of this experiment do not exclude a short-term IR-RF signal fading, but the experiment raised further questions about the reliability and reproducibility of the measurement system. Moreover, the IR-RF emission process cannot explain the observed differences in the IR-RF signal intensities.

Therefore further experiments were carried out with the goal of discovering the reasons for the observed phenomenon.

## 4. Isolating instrument effects on results

### 4.1. Hypotheses

Assuming that a sudden change in the IR-RF intensity cannot be explained by the underlying physical IR-RF stimulation and emission processes, the observations need to be attributed to the used measurement system (software/hardware). Considering the design of the *lexsys research* system (Richter et al., 2013), we hypothesised that the sudden change in the IR-RF sensitivity might have the following sources:

- A change in detection efficiency caused by the hardware (e.g., saturation effect in the PMT),
- a change in detection efficiency caused by the control software (e.g., buffer overflow),
- a change in the measurement geometry,
- a combination of reasons mentioned above.

We did not further investigate a change in detection efficiency caused by the control software since we did not have access to the source code of the *lexsys research* control software. For the geometry change a further distinction can be made between (A) a drift of the sample carrier on the sample arm (cf. Appendix: Fig. 13 for a technical drawing showing

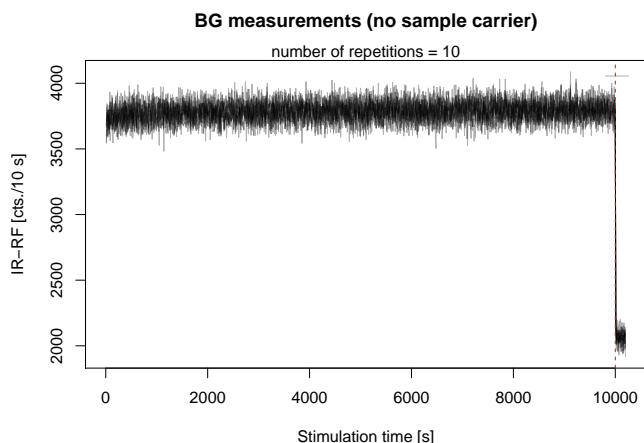


Figure 4. IR-RF background measurements without sample carrier and without load and unload step. The dashed red line indicates the closing of the shutter in front of the irradiation source.

the setup in the measurement chamber) and (B) an inaccurate sample arm positioning.

## 4.2. Background measurements

To test the overall reliability and reproducibility of the irradiation and the detection system, our first experiment aimed at repeatedly measuring the IR-RF background without a sample carrier on the sample arm and without a load and unload cycle in between. Therefore the sequence was modified manually after being created with the Freiberg Instruments *LexStudio2* software and consisted of the steps listed in Table 2.

Table 2. Background measurements without sample carrier and without load and unload step.

#	Step	Obs.
1	IR-RF for 10,100 s at room temperature, last 100 s: closed shutter	IR-RF
2	Pause of 60 s under the SLS position	-
3	Return to step 1	-

The last 100s were recorded while the shutter in front of the  $\beta$ -source was closed (red dashed line). The measurements were repeated ten times. The results are shown in Fig. 4. Due to technical limitations, the pause of 60s was not recorded and is not shown in the figure.

The measurements overlap and therefore cannot be distinguished in the figure. The results indicate a stable and reproducible IR-RF background with no sudden sensitivity change. This experiment was repeated with the following modified settings: (A) IR-RF for 1,000s, 20 repetitions and (B) with an empty sample carrier and the sample arm under the source for 10 s, with load and unload cycle, 70 repetitions. All experiments gave consistent results and are not further reported. To summarise, the background measurements (with and without sample carrier) indicated no apparent technical problem, but showed a highly reliable and sta-

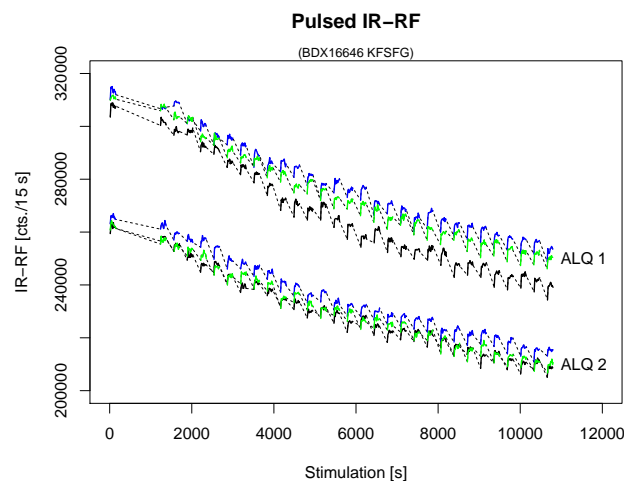


Figure 5. Pulsed IR-RF measurements. Colours indicate repetitions, the dashed line the applied real pause times.

ble system.

## 4.3. Pulsed IR-RF measurements

Pulsed IR-RF measurements aimed at constructing a consecutively recorded presumed continuously decaying IR-RF curve, similar to the one shown, e.g., in Fig. 1. Except for the first channel (opening of the shutter), the combined pulsed IR-RF curve increments should result in a curve similar to a continuously recorded IR-RF curve. For the experiment, we used the previously measured FG-KFS sample (BDX16646). The sample was bleached before measuring using the internal SLS for 10,800s, following the recommendations made by Frouin et al. (2017) (cf. Table 1, step 1). The sequence is listed in Table 3. 150s of stimulation are followed by a pause of 1s plus the time needed for the closing of the shutter located in front of the irradiation source. The stimulation-pause-cycle was repeated 30 times. Two aliquots were measured for one experiment, and the experiment was repeated three times. The results are shown in Fig. 5. The dashed lines indicate the applied pause under the irradiation source. No sample arm movement was assumed between the pause and the IR-RF measurements.

Table 3. Pulsed IR-RF sequence.

#	Step	Obs.
1	IR-RF measurements at 70 °C for 150 s, temperature stabilisation prior stimulation for 900 s	IR-RF
2	Pause of 1 s under $\beta$ -source	-
3	IR-RF measurements at 70 °C for 150 s, no temperature stabilisation	IR-RF
4	Pause of 1 s under $\beta$ -source	-
5	Return to step 3	-

The results reveal several unexpected effects.

- According to the sequence design the pause between each new IR-RF measurement should be 1 s. Instead, the time varied between 174s and 179s,

- the pause between the first and the second IR-RF signal appears to be even much longer,
- for all signals recorded during the 150 s intervals the intensity of the 1<sup>st</sup> channel was lower than for the 2<sup>nd</sup> one,
- the intensities recorded during the intervals show the expected decaying trend, but intensity levels vary considerably between subsequent intervals.

The long pause between the IR-RF measurements is the most striking observation. This pause is caused by a movement of the sample arm between each IR-RF step. After the pause of 1 s under the closed  $\beta$ -source, the sample arm moved to the SLS position and from there for an internal recalibration to the calibration position (located between the maintenance position and TL-extra position, cf. Richter et al. (2013), before finally moving back to the irradiation position. Additionally, the photomultiplier tube (PMT) was switched off after each IR-RF measurement and restarted, including a temperature stabilisation phase, before any IR-RF signal detection (Andreas Richter, personal communication, March 2017). The time needed for the sample arm re-calibration and/or the temperature stabilisation of the PMT varies by a few seconds so that the effective pause between *all* IR-RF measurements varied between 174 s and 179 s. The pause between the first IR-RF measurement and the following one was attributed to a faulty set timestamp in the XSYG-file and thus is not real. The lower signal intensity of the first channel is attributed to the movement of the shutter in front of the irradiation source (approx. 100 ms; cf. supplement Frouin et al., 2017).

Further tests were carried out to determine whether the variation of the IR-RF signal intensity correlates with either the (A) on/off cycle of the PMT or (B) the sample arm movement itself.

#### 4.3.1 Pulsed IR-RF - variation 1

To investigate the influence of the PMT run mode (on/off vs. continuous) and the sample arm movement (stopped vs. moving) on the IR-RF signal, the hardware control configuration file was modified manually. To consecutively exclude factors influencing the measurements, four different measurement modes were tested:

1. PMT mode: on/off | sample arm: moving
2. PMT mode: continuous | sample arm: stopped
3. PMT mode: on/off | sample arm: stopped
4. PMT mode: continuous | sample arm: moving

Setup #1 had already been tested in the previous experiments and was thus not repeated. Measurements with modes #2 to #4 were based on the pulsed IR-RF experiment described above (Table 3) using the same sample BDX16646 (FG-KFS). Before measuring the sample was reset using the internal SLS (similar bleaching settings as described above). The same aliquot was used for all experiments. The signal was not reset between each measurement. However, every new measurement mode required a reset of the reader

hardware, i.e. every test was interrupted by a full system re-initialisation.

The results of the experiments are combined in Fig. 6, the dashed line indicates pause times. Green and red lines distinguish data measured without (#2 and #3) and with (#4) movement of the sample arm. Similar to Fig. 5 the time passed between the first and the second cycle is an artefact of the data format.

Figure 6 is divided into three areas, separating modes #2, #3 and #4. Figure 6-#2 shows data recorded with the PMT in continuous mode and without movement of the sample arm. Pauses between stimulation cycles were fixed at 5 s and only the shutter of the  $\beta$ -source was closed between cycles. The channel resolution was 15 s/channel, i.e. 10 data points were recorded during each 150 s interval and the pause of 5 s cannot be observed in Fig. 6-#2. The results do not reveal any sudden sensitivity change. Due to the off/on cycle of the PMT in mode #3, including temperature stabilisation, the recorded time between each cycle increased to 75 s. The IR-RF curves in Fig. 6-#3 show no considerable intensity change, indicating a high stabilisation and constant detection efficiency of the PMT. In contrast, mode #4 (Fig. 6-#4) included movement of the sample arm and the time between each IR-RF cycle increased to ca. 170 s. Our data show that for this experiment the IR-RF curves vary markedly for each cycle. Instead of an expected signal decrease of ca. 3% from the 4<sup>th</sup> to 5<sup>th</sup> cycle, the IR-RF signal increases first by ca. 3% (6<sup>th</sup> cycle) and by another 4% for the 7<sup>th</sup> cycle. To increase the number of observations this experiment (setup #4) was repeated for 31 cycles, giving similar results (not shown).

These results indicate that the (1) on/off cycles of the PMT have no measurable influence on the signal intensity. The results also indicate that the unexpected IR-RF signal intensity changes are correlated with the movement of the sample arm and are caused by a change in the measurement geometry. Nevertheless, the results cannot reveal whether the geometry change is a product of an incorrect and varying sample arm positioning under the  $\beta$ -source or a movement of the sample carrier and/or the sample material itself triggered by the sample arm movement. To cancel out the one or the other possibility we performed another pulsed IR-RF experiment.

#### 4.3.2 Pulsed IR-RF - variation 2

In the *lexsyg research* reader(s) operated at the IRAMAT-CRP2A the heating element is covered by a stainless steel plate, which is fixed by three screws (cf. Fig. 7). A custom made sample carrier ('teddy-bear' sample carrier), was mounted on the plate covering the heating element on the sample arm (Fig. 7) and fixed with two screws to prevent a movement of the sample carrier on the sample arm.<sup>3</sup>

The original experiment listed in Table 3 was repeated

<sup>3</sup>Please note the here described experiments are highly experimental, using non-automatised, manual settings. The manufacturer recommends none of these experiments, and wrong settings can seriously damage the measurement hardware.

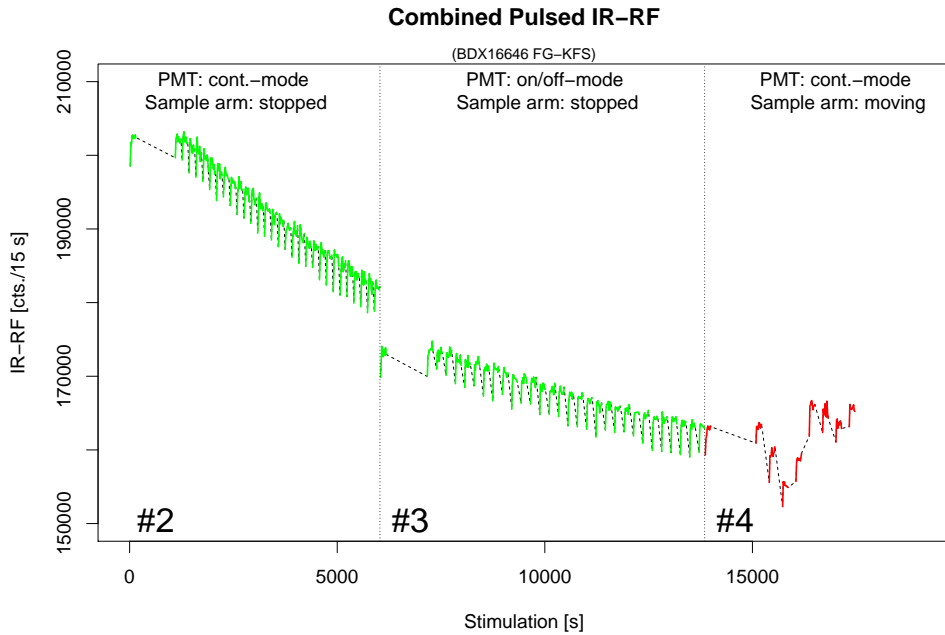


Figure 6. The figure shows a combination of three different pulsed IR-RF measurements. (#2) The PMT was operated in a continuous mode and the sample arm was not moving between each IR-RF cycle. (#3) The PMT was switched off and on between each shutter closing; the sample was not moving. (#4) The PMT was running in continuous mode, but the sample arm was allowed to move between each IR-RF simulation cycle. All measurements were carried out on one aliquot of the FG-KFS fraction of sample BDX16646. Dashed lines indicating passed time between each cycle. The dotted-dashed line separates the three different experiments. Colours emphasise the results. For further details see main text.

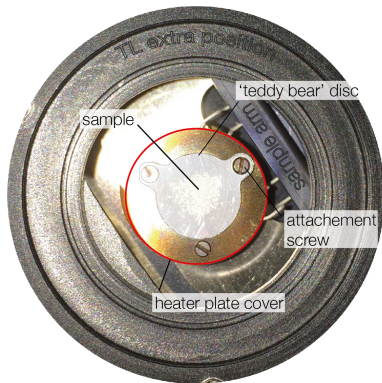


Figure 7. Photo of the sample arm with the heating plate and the special sample carrier ('teddy-bear' disc) fixed on the top. The picture was taken at the TL extra position Richter et al. (2013).

with this 'teddy-bear' disc. No other changes to the measurement settings were applied, i.e. the sample arm was allowed to move between each IR-RF cycle and the PMT automatically switched off and on. To be able to track individual grains, the natural coarse grain (100-200  $\mu\text{m}$ ) KFS fraction of sample BDX16646 was used instead of the bleached fine grain KFS fraction.

The grains were attached to the disc using silicon oil and a 4mm mask. No SLS bleaching was applied. Results of this experiment are shown in Fig. 8. No unexpected IR-RF intensity change was observed during the IR-RF cycles. From this observation, we conclude that the believed geometry change is not related to a wrong positioning of the sample arm it-

self but a movement of the sample carrier on the sample arm. Photos of the sample carrier were taken before and after the experiment. No unwanted grain loss or grain movement on the disc is observed if silicon oil is used.

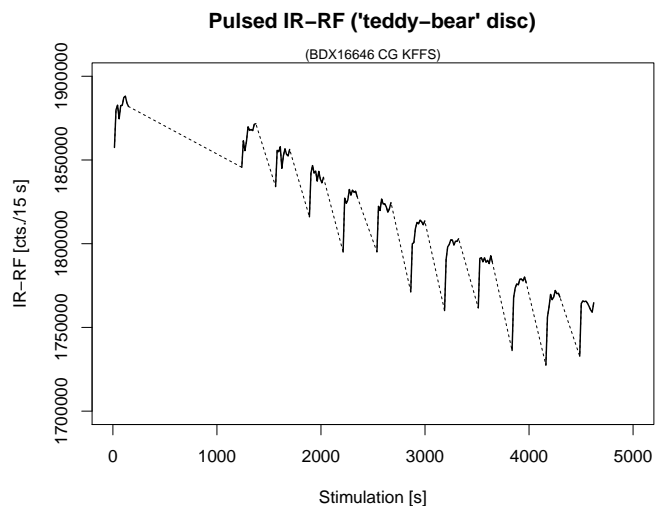


Figure 8. Results of pulsed IR-RF measurements on the coarse grain fraction of sample BDX16646 using a special sample carrier ('teddy-bear' disc). The disc was manually fixed on the stainless steel plate covering the heating element of the sample arm. The dashed lines indicate the real pause between each IR-RF measurement, except the first pause, which is data format artefact.

#### 4.4. Varying heating temperature

Figures 5, 6 and 8 show that intensity of the first IR-RF cycle is always slightly lower than it would be expected from the overall trend of the signal decay. The first cycle differs from the others due to the additional temperature stabilisation over 900 s (Table 1) under the closed shutter of the  $\beta$ -source (administered dose due to Bremsstrahlung ca. 1 mGy). Such stabilisation was not carried out for the subsequent cycles, where the heating element was allowed to passively cool down before the temperature was increased again to 70 °C. Due to the high thermal inertia of the heating element, the measured temperature between the IR-RF curves was never lower than 60 °C.

To ensure that our conclusions were not biased by unwanted changes of the stimulation temperature, we conducted an experiment varying the applied measurement temperature. Therefore, the heating ramp was actively modulated allowing temperatures between 50 °C and 90 °C (cf. Fig. 9). The IR-RF signal of sample BDX16646 (fine grain, KFS) was recorded continuously. Prior to measurement, the sample was reset using the internal SLS.

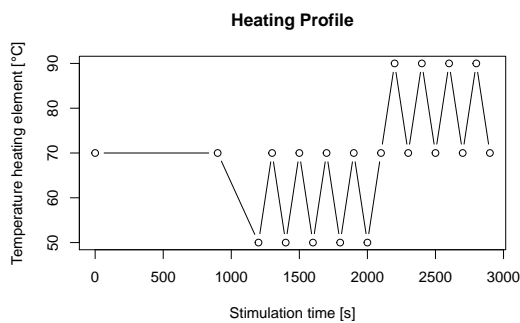


Figure 9. Preset heating profile as used for the 'varying heating temperature' experiment. After a stabilisation phase of 900 s the temperature is alternated between, (1) 70 °C and 50 °C and (2) between 70 °C and 90 °C.

Figure 10 (upper) shows the recorded IR-RF signal (black curve, 'NIR PMT'), the lower plot shows the temperature of the heating element recorded by the internal sensor in the heating element (red curve, 'Heating element'). The IR-RF detection started after a temperature stabilisation phase of 900 s (dashed line marked with '1'). Initially, the IR-RF signal remained stable even when the temperature was lowered to 50 °C, but dropped with a small delay while the temperature was increased again to 70 °C ('2'). The following IR-RF signals decrease sharply if the temperature is lowered and increase if the temperature is increased ('3', '4', '5'). The strongest decrease was observed after the temperature was first increased to 90 °C ('4') and then lowered to 70 °C ('5'). In contrast, for the experiments presented in Section 4.3 the maximum temperature was limited to 70 °C ('2'). The results show that temperature variations influence the IR-RF signal (e.g., Frouin, 2014). However, they cannot explain the observed light level changes, caused by the geometry change, but the chosen test sequence may have introduced an additional data scatter.

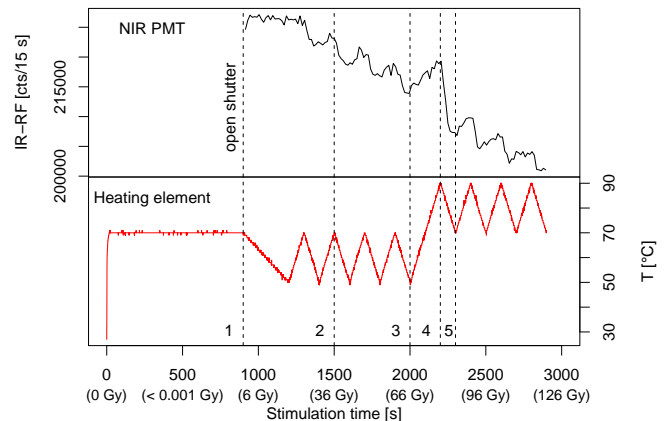


Figure 10. Results of the varying heating temperature experiment. The upper plot shows the recorded IR-RF signal and the lower plot the recorded temperature of the heating element (not the sample) using an internal sensor. Dashed lines and numbers in the plot label observations. The 2<sup>nd</sup> x-axis indicates the administered dose in Gy. For details see main text.

## 5. Discussion and further implications

Our findings demonstrate that the observed variation of the IR-RF signal intensity can be attributed to a change in the sample geometry. This geometry change appears to be induced by a movement of the sample carrier on the sample arm during its movement from one position in the reader to another. Krbetschek et al. (2000) considered the individual grain composition (non-emitting, less emitting grains) of each aliquot as the main factor for inter-aliquot scatter. Additionally, Erfurt (2003), Erfurt & Krbetschek (2003) and Erfurt et al. (2003) emphasised the general importance of a stable sample geometry. The original IRSAR protocol by Erfurt & Krbetschek (2003) explicitly demands a bleaching without geometry changes, but without giving further details, e.g., thresholds for allowed (or not allowed) geometry changes. For the investigated *lexsyg research* reader the general sample geometry appears to be unchanged, and the sample arm positioning seems to be precise. Nevertheless, our experiments revealed that the sample carrier does not remain stable on the sample arm causing a drop or a rise in the signal intensity from IR-RF cycle to IR-RF cycle.

### 5.1. What type of movement?

The question remains what type of movement occurs. The technical design (cf. Fig. 7) allows the sample carrier to drift laterally up to 0.5 mm, depending on the diameter of the sample carrier. The drift is limited by the screws on the metal plate covering the heater. Another possibility is a rotation of the sample carrier, which is potentially unlimited. To investigate the type of movement, photos of marked sample carriers on the sample arm were taken between arm movements. These experiments were performed on the *lexsyg research* systems at the IRAMAT-CRP2A in Bordeaux (France) and at the Justus-Liebig-University of Giessen (Germany). The results indicate that the sample carrier is likely to rotate and drift (Fig. 11).

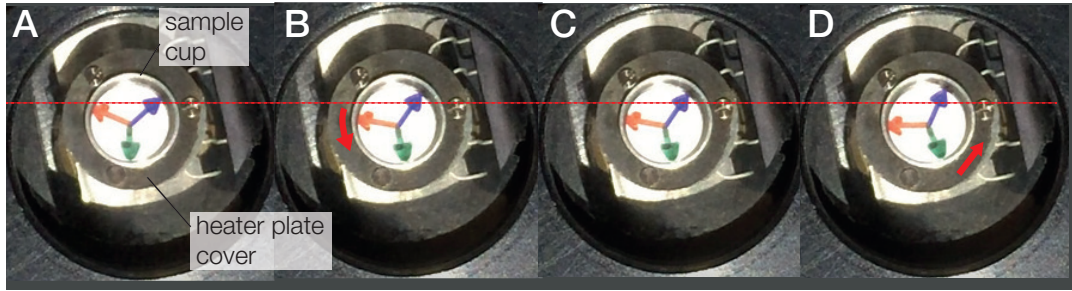


Figure 11. A set of four subsequent photos (A to D) taken of the sample arm holding a cup. The experiment was conducted with the *lexsyg research* reader 'Gauss' at the luminescence laboratory in Giessen. A paper with three arrows was placed on a standard sample cup. Red arrows indicate the movement of the sample carrier. Between each picture the sample arm was moved automatically by the reader. Between picture (A) and (B) the cup rotated slightly counterwise. No movement was observed from (B) to (C), while the cup slid upwards without rotation between (C) and (D).

## 5.2. Reasons for the movement

It is a tedious task to identify the reason for the movement beyond doubt, since the reasons may differ from reader to reader, and some of the systems might be not affected at all. For example: After its first weeks of operation, the system in Bordeaux suffered from a vibration of the sample arm. This issue was solved by a change of the drive chain. Such vibration can cause a drift of the sample carrier. Nevertheless, no vibration of the sample arm was observed for the *lexsyg research* readers in Giessen and Bordeaux in the course of these experiments.

Excluding this potential error source, it appears more likely that the drift and rotation of the sample carrier are favoured by a *combination* of two factors: (I) the radial movement of the sample arm (radial acceleration) and (II) a temperature-induced tension and bending of the metal plate covering the heating element. The heating element and the metal plate are made out of different materials (Andreas Richter, personal communication, March 2017). Differing thermal expansion coefficients force a faster expansion of the metal plate, which is fixed by the attachment screws. This setting is likely to cause a bending of the metal plate, producing a pivot point. If the sample arm starts the radial movement, the sliding friction is lowered, and the sample carrier can drift and/or rotate. In Bordeaux, the sample arm was removed from the reader for inspection and the bending of the covering metal plate has been confirmed.

The resulting sample carrier movement may appear small in absolute units ( $\leq 0.5$  mm), but is significant concerning the typically measured grain size ( $4 \mu\text{m}$  up to  $250 \mu\text{m}$ ). Whether the observed effect correlates with the grains size has not been tested.

## 5.3. Impact

Our results proved an intensity change caused by the sample carrier movements. However, the final impact on the  $D_e$  cannot be easily quantified. It depends on the IR-RF curve shape of a sample and the position of the observed light level on the curve. In other words, the impact in absolute terms is higher if the observed signal is close to saturation. In Fig. 12

we try to provide an estimate of the impact of a particular relative change of intensity caused by the measurement equipment on the final  $D_e$ . The parameters for the shown IR-RF curve were obtained via curve fitting from the  $R_{F_{\text{nat}}}$  curve shown in Fig. 1. Figure 12A simulates the impact of a 5% intensity change for a normalised intensity of 0.84 (max. 1). Assuming that the unbiased  $D_e$  has an arbitrary value of 2935, an increase of the light level (no curvature change) would result in a  $D_e$  of 1908 (ca.  $-35\%$ ) and 4414 (ca.  $+50\%$ ) for a light level decrease, respectively. Figure 12B shows the relative impact on the  $D_e$  for five different levels of intensity changes (isolines).

The simulations demonstrate the curve shape caused leverage effect of a few percent of intensity variation on the final  $D_e$ . Thus, even minor intensity changes have a significant impact on the final  $D_e$  and should be avoided.

## 5.4. Correction approach

An important other question is whether and how the encountered effect can be corrected. An obvious solution would be a re-design by the manufacturer to maintain a stable sample geometry. Freiberg Instruments have already developed a new heating element without any covering metal plate. This re-design has been subject to preliminary tests in Freiberg (Germany) using a *lexsyg research* provided by the manufacturer. For the tests three different types of sample carriers: Al cups, stainless steel cups (henceforth VA) and Ni cups were placed on the re-designed sample arm. Photos were taken after each movement of the sample arm. No sample carrier movement was observed for Al cups and Ni cups. In contrast, VA cups (similar to the cups used in Bordeaux and Giessen) still showed a considerable movement (rotation and drift). Hence, the used VA sample carriers were re-polished to remove any irregularities in thickness, and the tests were repeated. However, the procedure could not reduce the sample carrier movement, which indicates that the used VA sample carriers suffer from distortion stress. To overcome this problem the production process of the carriers must be modified. According to Freiberg Instruments, future plans include stress relief annealing during the produc-

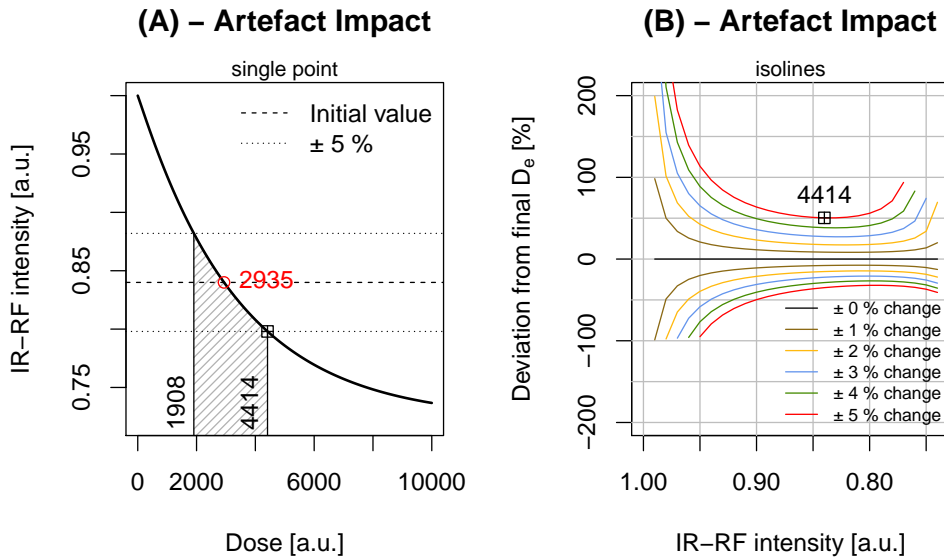


Figure 12. Impact simulation of light level changes on the final  $D_e$ . (A) The grey shaded area indicates the impact on the final  $D_e$  if the IR-RF intensity is increased (1908) or is decreased (4414) by 5%. (B) Isolines showing the expected relative deviation from the 'unbiased'  $D_e$  for different percentages of light level change. The crossed rectangle in both curves marks a similar change of light level and its impact in both plots. Both figures based on curve parameters obtained via fitting from sample BDX16646 FG-KFS and are limited to them. For further details see main text.

tion process (Kay Dornich, personal communication, March 2017).<sup>4</sup>

Until these changes have been made, we tested a data post-processing approach. Three assumptions were made:

- The change in the luminescence intensity is caused by a focus change under the PMT, i.e. the emission is dominated by different grains (of the sample aliquots),
- the IR-RF signal shape is not significantly affected due to an averaging effect of the multiple grain aliquot,
- bleaching and irradiation are homogeneous over the area of the metal plate.

The net effect would be a change in detection sensitivity without a change in the IR-RF signal shape. These assumptions allow for a vertical sliding of the  $RF_{nat}$  curve instead of only a horizontal sliding as suggested previously (Frouin et al., 2017). In other words, to obtain the  $D_e$  of a sample the  $RF_{nat}$  curves were moved horizontally and vertically (x- and y-direction, but no rotation) until the best match with the  $RF_{reg}$  was found. The new position which was obtained by searching the global minimum for the squared residuals from  $RF_{nat}$  and  $RF_{reg}$  was taken as best fit of both curves.

We tested this approach with the curves from Fig. 1. For the red curve of samples BDX16646 (FG-KFS) this correction results in an apparent dose of  $9 \{Q_{2.5}: 7.2 ; Q_{97.5}: 108\}$  Gy (red curves), instead of  $49.5 \{Q_{2.5}: 49.0 ; Q_{97.5}: 54\}$  Gy (red curves). The results of the black curve  $RF_{nat}$  (Fig. 1 left plot) remained unchanged. Although the expected dose was 0 Gy, the inter-aliquot scatter was reduced markedly by ca. 80%.

<sup>4</sup>Later tests carried out by Freiberg Instruments showed no sample carrier movement for the new setup even for VA cups. However, this could not further be verified before the manuscript was finished.

We further re-analysed the samples investigated by Frouin et al. (2017) and we found, except for sample BT706 ( $20.3 \pm 3.5$  ka instead of  $28.2 \pm 8.7$  ka) no 'improvement' of the ages towards a better match with the independent age control. All other results remained similar within errors, but the coefficient of variation (inter-aliquot scatter) was reduced in 6 out of 9 cases by 3% for sample FER3 up to 49% for sample BT706. Thus, it appears that a correction by vertical sliding may partly help to reduce the inter-aliquot scatter and correct for the above-described signal intensity change. The remaining inter-aliquot scatter may be attributed to natural grain variation as suggested by Krbeitschek et al. (2000) and supported by a study on single grains by Trautmann et al. (2000).

## 5.5. Further implications

Our results show the overall importance of a stable sample geometry for measuring IR-RF. We, therefore, recommend cross-checking results obtained with automatic systems and pay attention to effects described above.

Furthermore, the presented experiments are limited to IR-RF measurements only. However, there is no reason to believe that the movement of the sample carrier only affects IR-RF measurements. Therefore, we cross-checked optically stimulated luminescence (OSL) quartz calibration measurements carried out between 2015 and 2017 using Risø calibration quartz batch 90. In total, the results of six machines available at the IRAMAT-CRP2A were compared: Two Risø TL/OSL DA20 (e.g., Bøtter-Jensen, 1997), two *lexsyg SMART* (Richter et al., 2015) and two *lexsyg research* readers; this includes the *lexsyg research* reader investigated in this study. We found no evidence for a higher coefficient of variation. Nevertheless, taking into account the small num-

ber of observations (total number of measured aliquots per system: 25 to 30) such an effect cannot be excluded. Therefore we recommend that each system is tested independently.

### 5.6. Limitations of this study

We investigated sample carrier movements on *lexsyg research* systems in Bordeaux, Giessen and (briefly) in Freiberg. On all tested systems, sample carrier movements were observed. However, for the system in Freiberg with the re-designed sample arm, the movement was limited to VA cups only. For the system in Giessen, the sample arm movement appeared to be slightly lower than for the system in Bordeaux. Nevertheless, the detailed IR-RF measurements presented here were only carried out on one system in Bordeaux. From re-analysed IR-RF measurements performed on the system in Giessen, we have no clear evidence for effects on the IR-RF signal itself. Furthermore, we did not investigate whether the sample carrier preparation (grain mounting: ‘monolayer’ vs. ‘multilayer’) might influence the observed change in signal intensity.

## 6. Conclusions

A non-systematic luminescence intensity change while measuring the IR-RF signal of K-feldspar was identified. The change leads to a higher inter-aliquot scatter in measured dose values. We identified a lateral shift (up to 0.5 mm) and/or a rotation of the sample carrier on the heater plate covering the heating element. We further conclude:

- Our experiments are limited to a particular *lexsyg research* reader installed at the IRAMAT-CRP2A.
- We observed sample carrier movements for *lexsyg research* readers at the luminescence laboratories in Bordeaux and Giessen. However, clear evidence for an effect on the IR-RF signal was observed for the reader in Bordeaux only.
- We tested a re-designed sample arm at Freiberg Instruments, which showed no sample carrier movement for Al and Ni cups, but still for VA cups. The movement of the latter is believed to be caused by distortion stress.
- The impact of the intensity change on a  $D_e$  is sample dependent and cannot be properly quantified. However, due to the stretched exponential curve shape, even minor intensity changes cause a significant impact on the  $D_e$ .
- We tested a data post-processing approach to correct for the unwanted IR-RF signal intensity change combining vertical and horizontal curve sliding. The method was capable of reducing the inter-aliquot scatter for the tested samples by 3% up to 49%. However, it remains unclear whether this approach is capable of fully correcting the observed change in signal intensity.
- No statistical evidence was found for a higher inter-aliquot scatter for OSL on the same reader, though further measurements are needed to confirm these results.

Finally, our results show that unwanted instrument effects are not always directly visible, but they are capable of considerably biasing measurement results. Thus, the increased complexity of the measurement systems demands a careful differentiation between system induced effects and sample properties.

## Acknowledgements

Our manuscript benefited considerably from constructive input by Ashok Singhvi and Regina DeWitt. The authors further thank Guillaume Guérin for cross-checking the irradiation source calibration results. We thank Andreas Richter for his support while modifying the stack of the *lexsyg research* reader enabling the conducted experiments and for discussing the results. Rico Schweigel carried out the tests with the re-designed sample arm. The work of Sebastian Kreutzer is financed by a programme supported by the ANR - n° ANR-10-LABX-52. Madhav Krishna Murari is supported by the German Research Foundation (DFG A/C: 62201694).

## Appendix

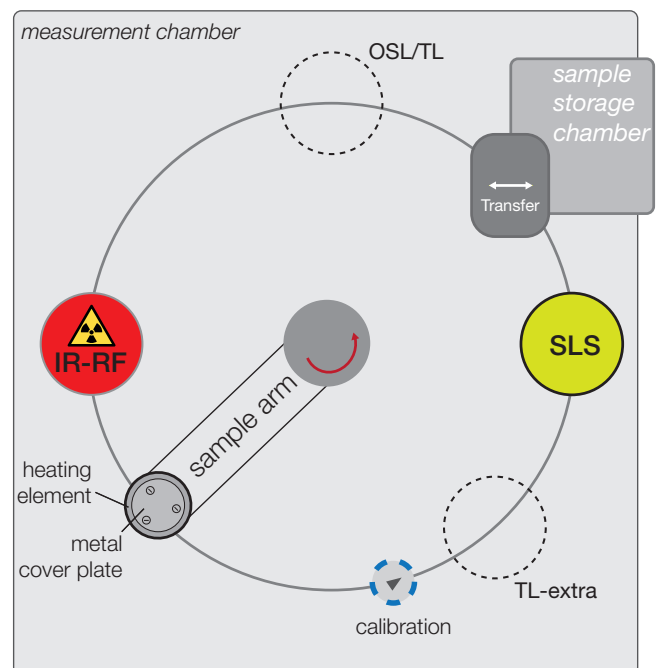


Figure 13. Technical drawing after Richter et al. (2013) showing the layout of the measurement chamber of a *lexsyg research* reader.

## References

- Adamiec, G., Heer, A., and Bluszcz, A. *Statistics of count numbers from a photomultiplier tube and its implications for error estimation*. Radiation Measurements, pp. 1–14, 2011.

- Bøtter-Jensen, L. *Luminescence techniques: Instrumentation and methods*. Radiation Measurements, 27(5/6): 749–768, 1997.
- Bray, H.E., Bailey, R.M., and Stokes, S. *Quantification of cross-irradiation and cross-illumination using a Risø TL/OSL DA-15 reader*. Radiation Measurements, 35(3): 275–280, 2002.
- Buylaert, J.P., Jain, M., Murray, A.S., Thomsen, K.J., and Lapp, T. *IR-RF dating of sand-sized K-feldspar extracts: A test of accuracy*. Radiation Measurements, 47(9): 759–765, 2012.
- Erfurt, G. *Radiolumineszenzspektroskopie und -dosimetrie an Feldspäten und synthetischen Luminophoren für die geochronometrische Anwendung*. PhD thesis, Technische Universität Bergakademie Freiberg, 2003.
- Erfurt, G. and Krbetschek, M.R. *IRSAR - A single-aliquot regenerative-dose dating protocol applied to the infrared radiofluorescence (IR-RF) of coarse-grain K-feldspar*. Ancient TL, 21(1): 35–42, 2003.
- Erfurt, G., Krbetschek, M.R., Bortolot, V.J., and Preusser, F. *A fully automated multi-spectral radioluminescence reading system for geochronometry and dosimetry*. Nuclear Instruments and Methods in Physics Research Section B: Beam Interactions with Materials and Atoms, 207(4): 487–499, 2003.
- Frouin, M. *Les feldspaths comme support pour la datation par luminescence de gisements archéologiques et de séquences quaternaires d'Aquitaine*. PhD thesis, Université Bordeaux Montaigne, France, 2014.
- Frouin, M., Huot, S., Mercier, N., Lahaye, C., and Lamothe, M. *The issue of laboratory bleaching in the infrared-radiofluorescence dating method*. Radiation Measurements, 81: 212–217, 2015.
- Frouin, M., Huot, S., Kreutzer, S., Lahaye, C., Lamothe, M., Philippe, A., and Mercier, N. *An improved radiofluorescence single-aliquot regenerative dose protocol for K-feldspars*. Quaternary Geochronology, 38: 13–24, 2017.
- Huot, S., Frouin, M., and Lamothe, M. *Evidence of shallow TL peak contributions in infrared radiofluorescence*. Radiation Measurements, 81: 237–241, 2015.
- Kadereit, A. and Kreutzer, S. *Risø calibration quartz – a challenge for  $\beta$ -source calibration. An applied study with relevance for luminescence dating*. Measurement, 46(7): 2238–2250, 2013.
- Krbetschek, M.R., Trautmann, T., Dietrich, A., and Stolz, W. *Radioluminescence dating of sediments: methodological aspects*. Radiation Measurements, 32(5-6): 493–498, 2000.
- Kreutzer, S. *Lab report: IR-RF and should we care about the a-value?* German LED 2016, 2016-11-04 to 2016-11-06, Emmendingen, Germany, 2016.
- Kreutzer, S., Schmidt, C., Fuchs, M.C., Dietze, M., Fischer, M., and Fuchs, M. *Introducing an R package for luminescence dating analysis*. Ancient TL, 30(1): 1–8, 2012.
- Kreutzer, S., Hülle, D., Thomsen, K.J., Hilgers, A., Kadereit, A., and Fuchs, M. *Quantification of cross-bleaching during infrared (IR) light stimulation*. Ancient TL, 31(1): 1–10, 2013.
- Kreutzer, S., Dietze, M., Burow, C., Fuchs, M.C., Schmidt, C., Fischer, M., and Friedrich, J. *Luminescence: Comprehensive Luminescence Dating Data Analysis*, 2017. URL <https://CRAN.R-project.org/package=Luminescence>. R package version 0.7.4.
- Lomax, J., Kreutzer, S., and Fuchs, M. *Performance tests using the lexsyg luminescence reader*. Geochronometria, 41(4): 327–333, 2014.
- Murray, A.S. and Wintle, A.G. *Luminescence dating of quartz using an improved single-aliquot regenerative-dose protocol*. Radiation Measurements, 32(1): 57–73, 2000.
- Preusser, F., Degering, D., Fuchs, M., Hilgers, A., Kadereit, A., Klasen, N., Krbetschek, M.R., Richter, D., and Spencer, J.Q.G. *Luminescence dating: basics, methods and applications*. Eiszeitalter und Gegenwart (Quaternary Science Journal), 57(1-2): 95–149, 2008.
- Richter, D., Pintaske, R., Dornich, K., and Krbetschek, M.R. *A novel beta source design for uniform irradiation in dosimetric applications*. Ancient TL, 30(2): 57–63, 2012.
- Richter, D., Richter, A., and Dornich, K. *lexsyg — a new system for luminescence research*. Geochronometria, 40(4): 220–228, 2013.
- Richter, D., Richter, A., and Dornich, K. *Lexsyg smart — a luminescence detection system for dosimetry, material research and dating application*. Geochronometria, 42(1): 202–209, 2015.
- Schmidt, C., Kreutzer, S., Fattahi, M., Bailey, R.M., Zander, A., and Zöller, L. *On the luminescence signals of empty sample carriers*. Ancient TL, 29(2): 65–74, 2011.
- Thomsen, K.J., Murray, A.S., Jain, M., and Bøtter-Jensen, L. *Laboratory fading rates of various luminescence signals from feldspar-rich sediment extracts*. Radiation Measurements, 43(9-10): 1474–1486, 2008.
- Trautmann, T., Krbetschek, M.R., Dietrich, A., and Stolz, W. *Feldspar radioluminescence: a new dating method and its physical background*. Journal of Luminescence, 85(1-3): 45–58, 1999.
- Trautmann, T., Krbetschek, M.R., and Stolz, W. *A systematic study of the radioluminescence properties of single feldspar grains*. Radiation Measurements, 32(5-6): 685–690, 2000.
- Wagner, G.A., Krbetschek, M.R., Degering, D., Bahain, J.-J., Shao, Q., Falguères, C., Voinchet, P., Dolo, J.M., Garcia, T., and Rightmire, G.P. *Radiometric dating of the type-site for Homo heidelbergensis at Mauer, Germany*. Proceedings of the National Academy of Sciences, 107(46): 19726–19730, 2010.
- Wintle, A.G. *Anomalous Fading of Thermoluminescence in Mineral Samples*. Nature, 245: 143–144, 1973.

## Reviewer

Ashok Singhvi, Regina DeWitt